Drug Delivery, 2010, 1–10, Early Online

informa
healthcare

RESEARCH ARTICLE

In vivo evaluation of novel chitosan graft polymeric micelles for delivery of paclitaxel

Jia Liu[1,2], Hongxia Li[1,3], Daquan Chen[4], Xiang Jin[1], Xiaoliang Zhao[1], Can Zhang[1], and Qineng Ping[1]

[1]College of Pharmacy, China Pharmaceutical University, Nanjing 210009, PR China, [2]Department of Pharmaceutical , The Northern Jiangsu People's Hospital, Yangzhou 225001, PR China, [3]School of Pharmaceutical Science, Jiangsu University, Zhenjiang Jiangsu 212013, PR China, and [4]School of Pharmacy, Yantai University, Yantai 264005, China

Abstract

A water-insoluble anti-tumor agent, Paclitaxel (PTX) was successfully incorporated into polymeric micelles formed from new graft copolymers, *N*-octyl-*N*-(2-carboxyl-cyclohexamethenyl) chitosan derivatives(OCCC). The objective of this study was to optimize and characterize the novel PTX micelle (PTX-M). Furthermore, the pharmacokinetics, NIR-imaging, biodistribution, and anti-tumor effects of PTX-M were evaluated. The results showed that the PTX-M had high drug loading (43.25%). The V_d and $t_{1/2\beta}$ of PTX-M were increased by 11.4- and 2.83-fold, respectively, but the plasma AUC of PTX-M was 3.8-fold lower than that of Taxol. Biodistribution study indicated that PTX-M was widely distributed into most tissues, most of them found in liver, spleen, lung, and kidney. This result was similar with NIR(near-infrared)-imaging. Tumor growth was significantly inhibited after intravenous injection of PTX-M. PTX-M showed the enhanced anti-tumor effect and non-toxic effects compared with Taxol, the commercial product of PTX. Therefore, the chitosan-derived micelle system offered a stable and effective platform for cancer chemotherapy with PTX.

Keywords: *Chitosan graft polymeric micelle; Paclitaxel; pharmacokinetics; NIR-imaging; biodistribution; in vivo anti-tumor effect*

Introduction

Paclitaxel (PTX), the first of a new class of microtubule stabilizing agents, has shown its potency against a broad spectrum of cancers, especially against non-small-cell lung cancer, metastatic breast cancer, and refractory ovarian cancer (Spencer & Faulds, 1994). However, paclitaxel is a hydrophobic molecule that is poorly soluble in water. Currently, one of the commercial formulations in clinical use (Taxol; Bristol Pharmaceuticals K. K., Tokyo, Japan) is an injection consisting of a solution of paclitaxel (6 mg/ ml) in a vehicle composed of Cremophor EL® (CrEL, polyoxyethylated castor oil) and ethanol at 50:50 (v/v) ratio. However, Cremophor EL® has been implicated in some adverse reactions when administered intravenously, such as hypersensitivity, nephrotoxicity, and neurotoxicity (Szebeni et al., 1998).

In order to eliminate the Cremophor EL®-based vehicle and increase the therapeutic efficiency, several attempts have been made to develop new drug delivery systems for PTX, including polymeric micelles (Huh et al., 2005; 2008; Torchilin, 2007; Lee et al., 2009; Li et al., 2009; Sawant & Torchilin, 2009; Huo et al., 2010; Liu et al., 2010; Zhu et al., 2010), Albumin-bound paclitaxel nanoparticle (ABI-007) (Ibrahim et al., 2002; 2005; Desai et al., 2006), liposomes (Crosasso et al., 2000; Yang et al., 2007; Sawant et al., 2010), microspheres (Liggins & Burt, 2004), nanoparticles (Matsumoto et al., 1999; Zhang & Feng, 2006; Zhang et al., 2010), PTX–polymer conjugates (Xie et al., 2007), and dendritic polymers (Ooya et al., 2003). Among them, polymeric micelles from amphiphilic graft or block copolymers were recognized as a promising nanocarrier system due to their characteristics such as reduced toxic side-effects of anti-cancer drug, passive

Address for Correspondence: Can Zhang, College of Pharmacy, China Pharmaceutical University, Nanjing 210009, PR China. Tel/Fax: (086)-025 83271171. Email: zhangcancpu@yahoo.com.cn

(Received 16 March 2010; revised 22 July 2010; accepted 30 August 2010)

ISSN 1071-7544 print/ISSN 1521-0464 online © 2010 Informa Healthcare USA, Inc.
DOI: 10.3109/10717544.2010.520355

targeting, solubilization of hydrophobic drugs, stable storage, long blood circulation, favorable biodistribution, reduced particle size, and low interactions with the reticuloendothelial system (RES) (Yokoyama et al., 1990; 1991; Kwon et al., 1993; Torchilin, 2001; Kwon, 2003). Furthermore, they had been evaluated in several clinical trials as carriers for anti-cancer drugs (Mizumura et al., 2002; Danson et al., 2004; Matsumura et al., 2004). In our group, *N*-octyl-*O*-sulfate chitosan (NOSC) micelles (Zhang et al., 2003; 2008b) and PEG-*N*-octyl-*O*-sulfate chitosan (PEG-NOSC) micelles (Qu et al., 2009) were reported to be safe and effective carriers for delivery of paclitaxel.

However, the problem of the polymeric micelle without adequate drug release upon micelle accumulation in the tumor tissues is usually revealed by clinical trials. Acidic pH is known to be a prominent microenvironment in solid tumors (Rapoport, 2007; Lee et al., 2008), so one approach to overcome the intracellular barriers is the application of pH-sensitive components that cause micelle destabilization in a specially controlled manner, thus increasing the selectivity and efficiency of drug delivery to target cells. Polymeric micelles formed by poly(ethylene glycol)-poly (aspartate hydrazide adriamycin) have been reported as effective drug delivery nanocarriers (Bae et al., 2007). Its response to intracellular acidic compartments such as endosomes and lysosomes resulted in the selective release of anti-cancer drug at low pH (< 6). Hruby et al. (2005) presented a novel pH-sensitive micelle drug delivery system based on hydrazone-bound doxorubicin (Hruby et al., 2005).

In early studies, we synthesized a series of novel pH-sensitive amphilic chitosan derivatives with long chain alkyl groups as hydrophobic moieties and amides with neighboring carboxylic acid groups as hydrophilic moieties for the solubilization of PTX (Liu et al., 2010). Among them, water-soluble graft polymer *N*-octyl-*N*-(2-carboxyl-cyclohexamethenyl) chitosan (OCCC) with 36.4% degree substitute (DS) of octyl showed the highest capacity in solubilization of PTX. Scheme 1 shows the structure of OCCC. In the previous report, physicochemical characterization and cell cytoxicities of PTX-M were

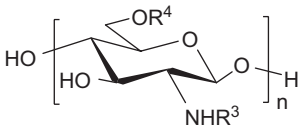

OCCC

R^3: –H, $–COCH_3$, $–C_8H_{17}$ or $–COC_6H_{10}COOH$

R^4: –H or $–COC_6H_{10}COOH$

Scheme 1. The chemical structure of *N*-octyl-*N*-(2-carboxyl-cyclohexamethenyl) chitosan (OCCC).

investigated. The polymeric micelles showed particle sizes ~ 145 nm in diameter and low critical micelle concentrations (CMC) ~ 42 μg/ml were found in the aqueous system. Besides, the drug release study showed that the pH sensitivity of PTX releasing from the micelle was caused by pH 5.5 and could overcome the intracellular barriers to improve the anti-tumor efficacy.

In the present study, we prepared PTX-micelles (PTX-M) and compared the pharmacokinetics, biodistribution, anti-tumor efficacy, and near-infrared (NIR) imaging with Taxol.

Methods

Materials

Paclitaxel was supplied by Taihua Natural Plant Pharmaceutical Co. Ltd. (China). Diazepam was obtained from Nanjing Xiandao Chemical Co. Ltd. (Jiangsu, China). *N*-octyl-*N*-(2-carboxyl-cyclohexamethenyl) chitosan (OCCC) was synthesized in our lab. All other chemicals were of analytical grade.

Sprague-Dawley (SD) mice and Kunming mice were obtained from Nantong University, BALB/cA nude mice were obtained from Yangzhou University. All the animals were pathogen-free and allowed to access food and water freely. The experiments were carried out in compliance with the National Institute of Health Guide for the Care and Use of Laboratory Animals.

Preparation and characterization of PTX-M

PTX-M was prepared by dialysis as described previously (Zhang et al., 2010). After selecting the appropriate chitosan derivative as the PTX-M carrier, the central composite design was used to optimize the preparation of PTX-M. OCCC (7.5 mg) and PTX (7.5 mg) were dissolved in 2.5 ml water and 0.25 ml ethanol, respectively. Then the PTX solution was dropped into OCCC solution with magnetic stirring at room temperature, and the mixture was dialyzed against distilled water overnight at room temperature using dialysis membrane (MWCO 10 kDa). The micelle solution was filtrated through a 0.22 μm pore-sized microfiltration membrane and lyophilized by a freeze dryer system (Songyuanhuaxing, China) to obtain the dried powder of PTX-M. The size and Zeta potential of the micelles were measured by dynamic light scattering (Zetasizer 3000 HAS, Malvern, UK).

The PTX concentration was analyzed by high-performance liquid chromatography (HPLC) method. The HPLC was equipped with a reverse-phase column (4.6 mm × 250 mm, Hanbon, Jiangsu, China) at 40°C and with a UV spectrophotometer (Agilent Technologies,

Palo Alto, CA). The mobile phase was a mixture of methanol and water (75:25 v/v). The samples were delivered at a flow rate of 1.0 ml/min and detected at a wavelength of 227 nm. A certain volume of PTX-M solution was taken and redissolved with 50-fold volume mobile phase, and 20 µl of dilution was injected into the HPLC system. The PTX-loading and entrapment efficiency in micelles were calculated by the following equations:

$$\text{drug-loading} = C \times V/(W_{\text{freeze–dried micelle}}) \times 100\% \quad (1)$$

$$\text{entrapment efficiency} = C \times V/(W_{\text{PTX}}) \times 100\% \quad (2)$$

where C, V, $W_{\text{freeze-dried micelle}}$, and W_{PTX} represent the PTX concentration of micelle solution, the volume of micelle solution, the weight of freeze-dried micelle, and the weight of PTX added, respectively.

DSC analysis was performed using the lyophilized powder with DSC-204 instrument (NETZSCH Ltd., Germany). The lyophilized powder of micelle, OCCC, PTX, and physical mixture of OCCC and PTX were put into a standard crucible, respectively. Heating temperature from 40°C to 300°C, heating rate was 10°C/min, the cooling nitrogen was 20 ml/min.

Pharmacokinetic studies of Taxol®, PTX-M in mice

Sprague-Dawley mice (220–260 g) were used to examine the pharmacokinetics of PTX-M. Mice were randomly divided into the following two groups ($n = 5$): (1) PTX-M (PTX dose: 7 mg/kg), (2) Taxol (PTX dose: 7 mg/kg). Drugs were intravenously injected through the tail vein. The blood samples (0.5 ml) were collected from the plexus venous in the eye ground at 5 min, 10 min, 30 min, 1 h, 2 h, 3 h, 4 h, and 8 h; 140 µl of blood sample, 10 µl of internal standard (Diazepam in methanol), and 290 µl of acetonitrile were added into a protein precipitation tube. The mixture was vortexed for 5 min and centrifuged at 8000 rpm for 10 min; 20 µl of the solution was injected onto the HPLC system. The HPLC was equipped with a reverse-phase column (4.6 mm × 250 mm, Hanbon, Jiangsu, China) at 35°C and with a UV spectrophotometer (Agilent Technologies, Palo Alto, CA). The mobile phase was a mixture of methanol and water (72:28 v/v). The samples were delivered at a flow rate of 1.0 ml/min and detected at a wavelength of 227 nm. Drug and Statistics for Windows (DAS ver 2.0) was utilized to analyze the pharmacokinetic parameters of the area under the plasma concentration time curve ($AUC_{0-\infty}$), the apparent volume of distribution (V_d), total body clearance (CL), distribution half life ($t_{1/2\alpha}$),elimination half life ($t_{1/2\beta}$), and mean residence time (MRT) of PTX for each formulation.

In vivo near-infrared (NIR) fluorescence imaging in mice

Preparation and optical characterization of NIRD-15-micelle and NIRD-15-Taxol

NIRD-15 (0.7 mg), a kind of hydrophobic dye with maximum absorption at 760 nm and maximum emission at 814 nm, was dissolved in ethanol. OCCC (12.0 mg) was dissolved in 4.0 ml water. After that, NIRD-15 solution was drop-wisely added to OCCC solution and the mixure was dialyzed against distilled water for 12 h. Then the green micelle solution was collected, filtrated through a 0.45 µm pore-sized microfiltration membrane.

NIRD-15-Taxol solution was prepared by adding 0.35 mg NIRD-15 into 2.0 ml cremophor EL® and ethanol at 50:50 (v/v). The amount of NIRD-15 in micelle and Taxol was detected by a UV–visible spectrophotometer.

Absorbance and fluorescence spectra of entrapped NIRD-15 in micelle and Taxol were measured by using a Lambda 35 UV–visible spectrophotometer (Perkin Elmer, USA) and S2000 spectrometer (Ocean Optics, USA), respectively. A NL-FC-2.0-763 semiconductor laser ($\lambda = 765.9$ nm, Enlight, China) was used to excite fluorescence. The photo stability of entrapped NIRD-15 in micelle and Taxol was evaluated by measuring their relative fluorescence intensity under continuous exposure to the laser for 2 h, with a 5 min interval for data acquisition.

In vivo animal test

The female naked mice were used in this experiment. Ten healthy mice were evenly divided into two groups; 200 µl of NIRD-15-micelle and NIRD-15-Taxol solution, for control (each containing 100 µg/ml of NIRD-15) was injected through the tail vein into the nude mouse. The dynamic behaviors of nanocarriers were monitored by a NIR imaging system, which were reported in Gu's group (Chen et al., 2008; Zhang et al., 2008c). Fluorescence images of all the experimental mice were taken continuously for 10 min and the typical images at 1 h after injection. Mice were sacrificed and images of separated tissues were taken to show the target ability of micelle at 8 h post-injection.

Tissue distribution studies

To assess the effect of micelle formulation on tissue distribution of PTX, mice (50% male and 50% female) were randomly divided into two groups ($n = 5$), Taxol and PTX-M. Taxol and PTX-M were intravenously administrated via tail vein at a dose of 20 mg/kg. After 0.25, 0.5, 1, 2, 4, 6, and 8 h of injection, blood samples were collected from the eyes of six mice in each group, after which the mice were sacrificed by cervical dislocation. Then the blood was immediately treated as described.

The organs (heart, liver, spleen, lung, and kidney) were collected and thoroughly rinsed in normal saline, then blotted dry and weighed. Subsequently, the weighted tissues were homogenized (Tearork, BioSpec Products Inc., Bartlesville, OK) with 2-fold weight of normal saline; 150 μl of homogenate, 10 μl of internal standard (Diazepam in methanol), and 290 μl of acetonitrile were added. The mixture was vortexed for 5 min and centrifuged at 15,000 rpm for 10 min; 20 μl of the supernatant was injected onto the HPLC system.

The concentrations of PTX in samples were analyzed under the conditions described. The parameters of blood, heart, liver, spleen, lung, and kidney were evaluated using the statistical moment method.

In vivo anti-tumor effect and histological studies

In vivo anti-tumor efficacy of PTX-M was evaluated with the animal tumor models set up by inoculation of mouse Heps cancer cell line. BALB/cA (18~22 g, male) was injected, which was inoculated subcutaneously with 1×10^6 mouse Heps cancer cell line. Treatments were started when the tumor in the mice reached a volume of 100~300 mm^3, this day was designated day 0. On day 0, mice were weighed and randomly divided into four groups ($n=5$): (1) negative control group (saline group); (2) Taxol (PTX dose: 20 mg/kg); (3) PTX-M (PTX dose: 20 mg/kg); (4) OCCC-blank (OCCC dose: 30 mg/kg, 40% drug loading, equivalent to the OCCC mount in PTX-M). The control saline or drugs were administrated via the tail vein at day 0, day 2, day 4, and day 6. At day 9, all the mice were weighted and sacrificed by cervical vertebra dislocation followed by separation and measurement of the tumor block. Tumor volume was calculated by the formula:

$$\text{Tumor volume} = \mu \times (W^2 \times L)/6 \quad (3)$$

where W is the tumor measurement at the widest point, and L is the tumor dimension at the longest point measured by a slide caliper. The anti-tumor efficacies of each formulation were evaluated by tumor inhibition rate (TIR, %), which was calculated from tumor weight at day 9, following the equation:

$$\text{TIR},\% = 1 - \frac{\text{Mean weight of tumor in treated group}}{\text{Mean weight of tumor in blank group}} \times 100\% \quad (4)$$

Separated tumor tissues were fixed in 10% formalin and embedded in paraffin, and then sections with 3 μm thickness were prepared. These thin sections were placed on glass slides, deparaffined in xylen, and dehydrated in graded alcohols. These slides were stained with hematoxylin and eosin (HE). Then all the slides were observed under a microscope.

Statistical analysis

Statistical comparisons were performed by Student's *t*-test for two groups, and one-way ANOVA for multiple groups. Values of $p<0.05$ and $p<0.001$ were considered statistically significant and highly significant, respectively.

Results and discussion

Preparation and characterization of PTX-M

The dialysis method was used to prepare drug-loaded micelle solutions based on chitosan derivates, and the drug-loaded micelle powder was obtained via lyophilization. The drug loading and entrapment efficiency could reach 31.47% and 44.05%, respectively. The micelle size and zeta potential were 145.9 ± 8.4 nm and −14.8 ± 0.6 mv, respectively. Then Doehlert matrix design (DMD) was used to optimize the conditions to prepare the PTX-micelle. Before using the design, a number of preliminary experiments were conducted to identify the control factors and their levels. Then a Doehlert matrix was used for optimization of three variables, the optimal feed ratio of OCCC and PTX was screened as 24/25 (W/W), the concentration of OCCC was 3.0 mg/ml, and the dialysis time was 6 h, enough to remove ethanol. Besides, the centrifugation process of the micelle was rejected, the resultant drug loading and entrapment efficiency increased obviously, achieving 41.85% and 65.45%, respectively.

DSC thermograms (Figure 1) revealed PTX had a fusion characteristic endothermic peak at 217.8°C. The endothermic peaks around 60~70°C of a, c, and d groups could be attributed to water loss of chitosan derivative (Wanjun et al., 2005). The exothermic peaks around 230°C of a, b, and c groups might be the characteristic peak of PTX decomposition. For physical mixture, the peak of PTX was observed with small shifts. The characteristic endothermic peak of lyophilized drug-loaded micelles around 217.8°C disappeared and exothermic peak was very low, which suggested that most of the PTX was encapsulated by micelles in the non-crystalline form.

Pharmacokinetic analysis of PTX-M after intravenous administration

The drug concentration was detected by HPLC analysis, which has been validated. The plasma concentration time profiles of PTX after intravenous administration of PTX-M and Taxol were shown in Figure 2. For PTX-M, the values of area under the plasma concentration time curve ($AUC_{0-\infty}$) was 3.90 μg/l/h, whereas the corresponding total body clearance (CL) was 1.89 l/kg. A rapid decline in concentrations of PTX in the micelle group represented a distribution phase, which was followed by an elimination

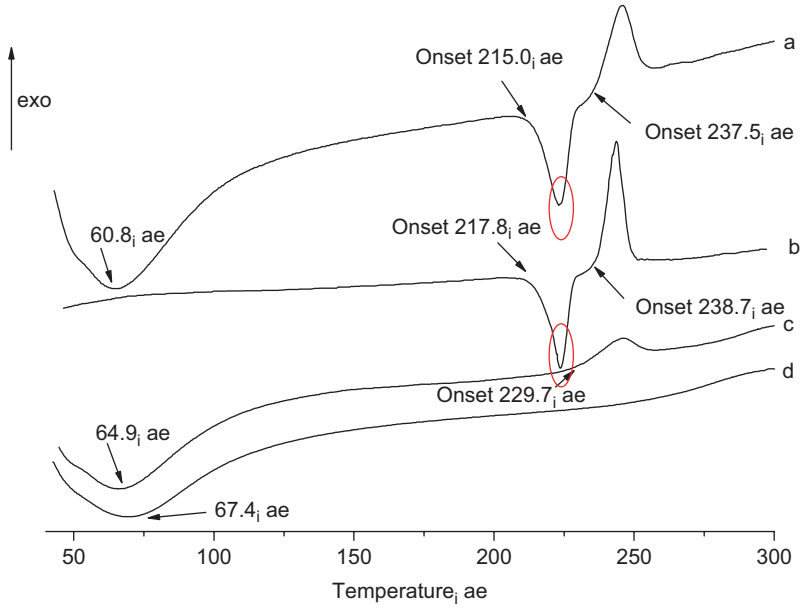

Figure 1. DSC spectra of (a) physical mixture of paclitaxel and OCCC (2:3(w/w)), (b) paclitaxel, (c) PTX-M (PTX-loading 41%), and (d) OCCC.

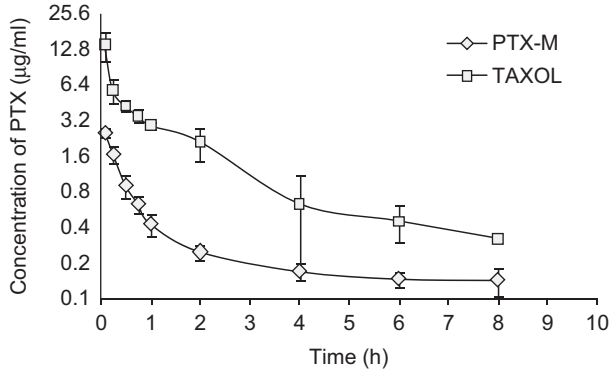

Figure 2. Time courses of PTX levels in mice plasma after i.v. administration of PTX-M and Taxol. Each point represents the mean ± SD ($n=5$).

Table 1. Pharmacokinetic parameters of PTX in the two formulations after i.v. administration.

Parameters	PTX-M	Taxol
V_d	2.06 ± 0.18**	0.18 ± 0.12
$t_{1/2\alpha}$	0.22 ± 0.04	0.13 ± 0.08
$t_{1/2\beta}$	5.31 ± 1.07	1.87 ± 0.32
CL	1.89 ± 0.30*	0.48 ± 0.06
$AUC_{(0-\infty)}$	3.90 ± 0.59**	14.85 ± 1.86
$MRT_{(0-\infty)}$	4.40 ± 0.53*	2.44 ± 0.06

Data represent mean value ± SD, $n=5$.
* $p<0.001$, ** $p<0.01$, compared with Taxol.
V_d, apparent volume of distribution; $t_{1/2\alpha}$, distribution half-life; $t_{1/2\beta}$, elimination half-life; CL, total body clearance; $AUC_{(0-\infty)}$, area under the plasma concentration time curve; MRT, mean residence time.

phase with $t_{1/2\beta}$ of 5.31 h. However, the plasma AUC of Taxol was 3.8-fold higher than that of the PTX-M; and the V_d, $t_{1/2\beta}$, and CL of PTX in Taxol were decreased by 11.4-, 2.83-, and 2.8-fold, respectively. It was reported that a similar phenomenon was observed in the research about PTX-loaded NOSC micelles in our group (Zhang et al., 2008a).

PTX encapsulated by micelles in plasma concentrations could be described by a two-compartment open model, and this model was similar to PTX in Taxol. As indicated in Table 1, after intravenous administration of PTX-M and Taxol, PTX in micelle was distributed from blood to tissues more quickly, resulting in the lower plasma AUC of PTX micelle. The larger V_d of PTX-M could explain this phenomenon. Moreover, it was reported that the CrEL in blood as large polar micelles with a highly hydrophobic interior may cause the non-linear pharmacokinetic process of PTX and was also attributed to the high blood accumulation of drug (van Zuylen et al., 2001). The innner core of micelle with weaker hydropobic interaction could't entrap drug ,which would result in the lower AUC of PTX in blood.

The higher $t_{1/2\beta}$ might be attributed to the long blood circulation effect of micelles. Furthermore, PTX in micelle releasing from tissue to blood during metabolism may increase the higher $t_{1/2\beta}$. It was reported that there was a large V_d in the pharmacokinetic research of paclitaxel (Sonnichsen & Relling, 1994). In our research of paclitaxel micelles in mice, a similar phenomenon of increased apparent volume of distribution was observed, suggesting that paclitaxel is most extensively distributed. Similar increases in volumes of distribution at steady state were previously reported for carrier-entrapped paclitaxel (Kim et al., 2001).

On the whole, the change in the biological fate of PTX led to a decrease in AUC, and an increase in CL and V_d for

the encapsulated drug clearly signify the role of a carrier system in influencing distribution of drugs in vivo.

Non-invasive NIR imaging

After intravenous administration of micelle, a rapid decline in plasma concentration was indicative of rapid distribution of drug into highly perfused organs, such as liver, lung, spleen, and kidney. Hence, non-invasive and real-time imaging systems can be effectively and conveniently employed to visualize and evaluate tissue distribution of drug carriers in vivo.

Figure 3 exhibited the typical fluorescence images of different group mice and separated tissues. Figures 3A(a) and B(a) showed that fluorescent signals were found in the liver at 10 min post-injection. So it was obvious that both micelle and Taxol were distributed to liver more quickly than other tissues; furthermore, the intension of fluorescent signal represented that the amount of micelle targeted to liver was more than the Taxol group. Compared with the signal of micelle at 10 min, the weaker fluorescent signal in liver at 1 h was found.

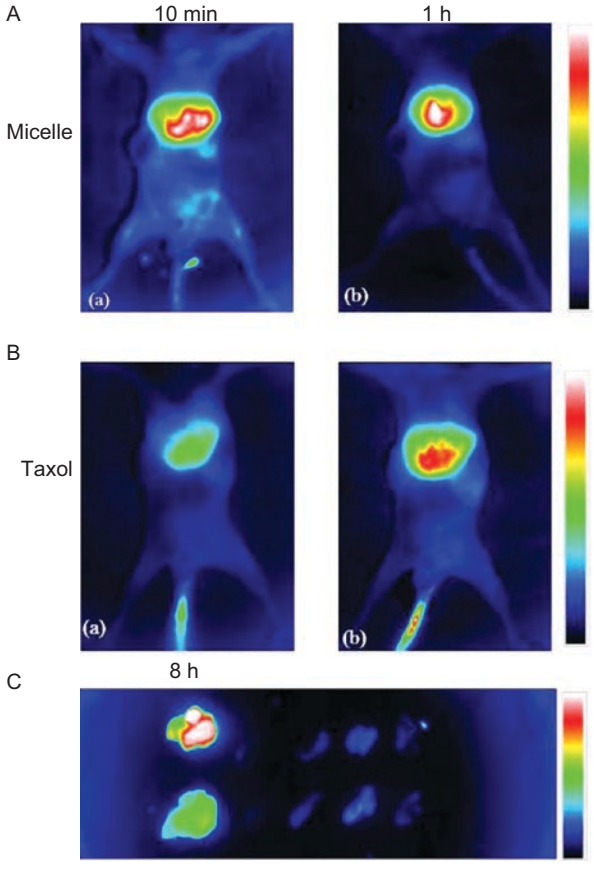

Figure 3. (A) NIR fluorescence imaging photos of NIRD-15- micelle: (B) NIR imaging photos of NIRD-15- Taxol solution; (C) Organ photos of micelle and Taxol group after 8 h (the upper is micelle group, lower is Taxol group. From left to right: liver, heart, spleen, kidney, and lung).

A bright fluorescent signal in liver of Taxol at 1 h (Figure 3B(b)) was observed and intension *y* of signal was stronger than that at 10 min (Figure 3B(a)). This demonstrated that much more NIRD-15 in Taxol was distributed into liver, which was consistent with earlier tissue distribution research. The fluorescence imaging was still obviously observed at 8 h post-injection for two groups (Figure 3C). The separated tissues after 8 h (Figure 3C) showed that the highest NIRD-15 signal was found in liver, lung, and spleen which was caused by the uptake by RES, then followed by kidney and heart.

Tissue distribution of PTX-M after intravenous administration

According to the result of NIR-imaging, the aim of the tissue distribution experiment was to quantify and identify the key factors influencing biodistribution of various drug carriers. The tissue distribution profiles of PTX-M and Taxol after intravenous administration were compared in mice. The concentration of PTX in blood and organs of heart, liver, spleen, lung, kidney after intravenous administration of 20 mg equivalent PTX/kg body weight for OCCC-micelle and Taxol, were presented in Figure 4. The observed PTX concentrations in blood and tissues were estimated to obtain the pharmacokinetic parameters by statistical moment analysis. The maximum concentration (C_{max}) (μg/ml or μg/g) and the time of maximum concentration (T_{max}) (h) values were obtained from visual inspection of the data. Table 2 summarized the AUC (0–t_n) and MRT (0–t_n) values of PTX in various tissues and blood.

As suggested in Figure 4, the concentration of PTX in blood after intravenous administration of micelle was much lower than PTX in Taxol. PTX was widely and rapidly distributed into most tissues following intravenous administration of PTX-M, and the highest concentration of PTX was found in liver, followed by kidney and lung at 5 min after administration. This characterization of targeted distribution was consistent with NIR-imaging exhibited in Figure 3; the highest PTX concentration in the liver of micelle was found at 5–10 min after administration. Moreover, tissue distribution studies of PTX-M were also consistent with the results reported by Rowinsky and Donehower (1993). The localization of PTX in the liver and lungs was caused by the uptake by RES. The similar result of biodistribution was observed in the research about micelle-based on chitosan derivatives (Zhang et al., 2008a; Qu et al., 2009).

It was reported that several factors, such as particle size, surface charge, molecular weight, blood circulation time, and cellular uptake, are responsible for determining nanoparticle body distribution and fate in blood (Cho et al., 2007). In our research, a considerable amount of PTX in micelle accumulated in kidney, which was a non-RES organ, suggesting that it may be the increased

kidney elimination of micelle. The kidney elimination was influenced by the solubility and hydrophobicity of carrier, the more soluble the carrier, the more easy the kidney elimination. This phenomenon was previously observed in water-soluble paclitaxel–prodrug, which resulted in the kidney elimination of drugs other than hepatic biotransformation (Dhanikula et al., 2005).

Importantly, compared with Taxol, lower AUC (0–t_n) values for PTX-M in the heart ($p<0.05$) were shown in

Table 2. AUC (0–t_n) and MRT (0–t_n) of Taxol, PTX-M in blood and tissues ($n=5$).

	AUC (0–t_n)[a] (h×μg/ml)			MRT[b] (0–t_n) (h)	
Tissues	PTX-M	Taxol	Re	PTX-M	Taxol
Blood	16.86	30.67	0.55	1.88	1.18
Heart	23.86	62.59	0.38	1.31	2.12
Liver	192.44	231.98	0.83	1.97	2.16
Spleen	15.54	70.73	0.22	1.47	2.39
Lung	37.65	103.90	0.36	2.35	2.28
Kidney	68.59	60.02	1.14	2.32	1.69

[a] The area under the plasma concentration–time curve from time 0 to the last time point examined.
[b] Mean residence time from time 0 to the last time point examined.
Re = AUC_{PTX-M}/AUC_{Taxol} = AUC (0–t_n) of PTX-M /AUC (0–t_n) of Taxol.

Table 3. In vivo anti-tumor effect of PTX-M, Taxol, and OCCC-blank in tumor-bearing mice model.

	Body weight(g)		Tumor	
Drug	Before i.v	After i.v	Weight (g)	TIR,%
saline	21.91 ± 0.07	25.00 ± 1.58	0.52 ± 0.12	—
OCCC-blank	23.58 ± 0.06	24.00 ± 2.55	0.45 ± 0.10	13.46
PTX-M	24.53 ± 1.17	24.00 ± 0.82	0.23 ± 0.08**	55.77
Taxol	24.59 ± 1.48	24.56 ± 0.25	0.31 ± 0.03*	40.38

Data represent mean value ± SD, $n=5$.
* $p<0.05$, ** $p<0.01$, compared with Normal saline group.

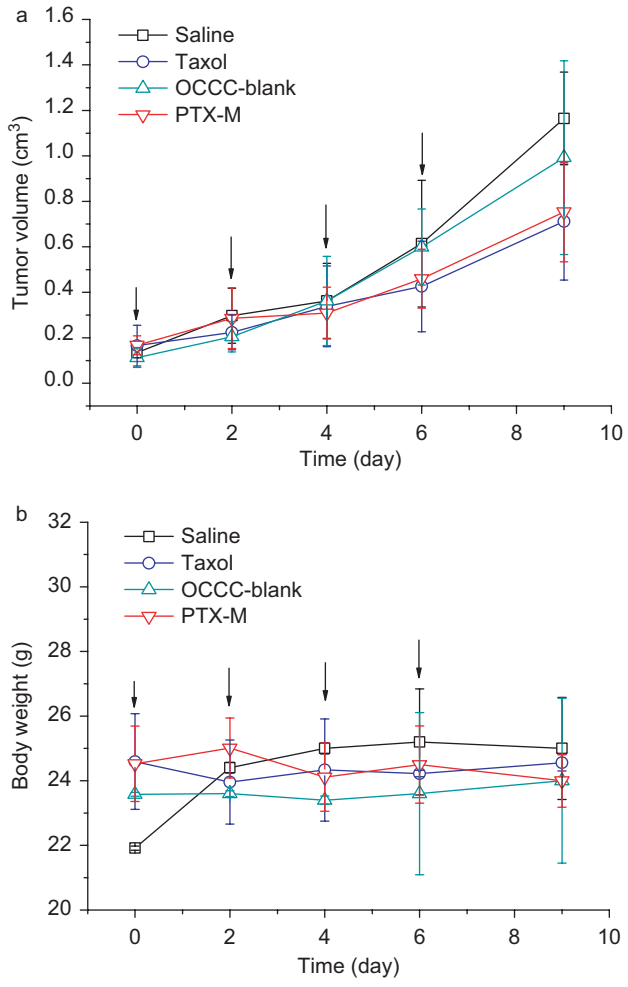

Figure 5. Body-weight change (a) and tumor volume change (b) in mice with PTX-M, Taxol, OCCC-blank, or saline four times (at arrows).

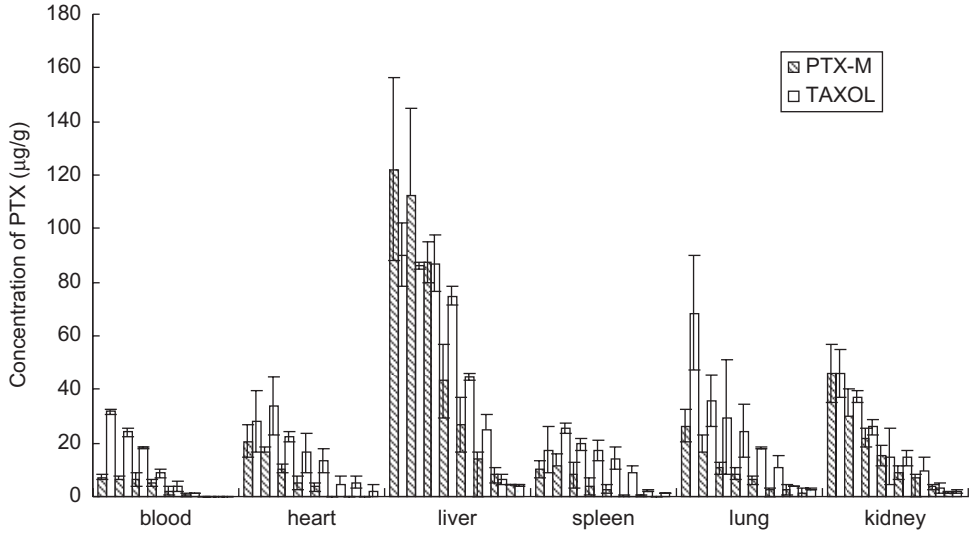

Figure 4. Comparison of PTX concentrations in mice receiving PTX-M or Taxol at different sample times (in the order of 5 min, 15 min, 30 min, 1 h, 2 h, 4 h, and 8 h). Each column represents the mean ± SD ($n=5$).

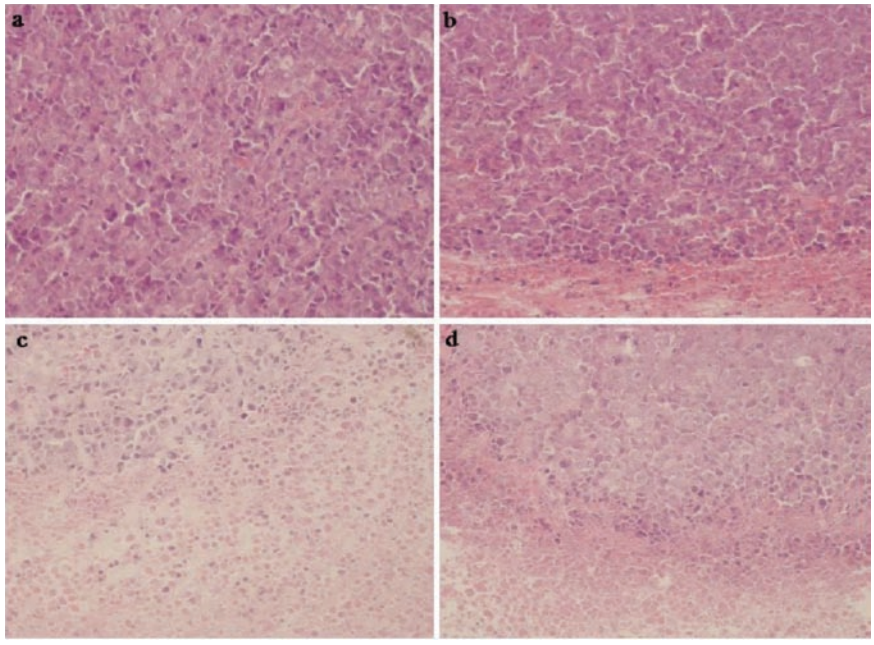

Figure 6. HE staining photos of tumor histological slides (×200 in the original) (a) saline group; (b) OCCC-blank group; (c) PTX-M group; (d) Taxol group.

Table 2, so micelle formulation could reduce accumulation of paclitaxel in the heart.

In vivo anti-tumor efficacy and histological studies

The in vivo anti-tumor efficacy of OCCC-micelle was evaluated in tumor-bearing BALB/c mice.

As shown in Figure 5, The tumor volume of the saline control and OCCC-blank group were excessively enlarged (~ 1000 mm^3), while other groups were much smaller. Compared with the saline control, the PTX-M and Taxol groups ($p < 0.01$) markedly inhibited tumor growth at day 9 and there was no significant adverse effects between the drug group and the saline group, such as body weight loss.

The data of body weight and tumor weight were summarized in Table 3. The tumor weight change after injection was consistent with above. Compared with saline control, PTX-M ($p < 0.01$) and Taxol ($p < 0.05$) markedly inhibited the growth of solid Heps tumor. The TIR at day 9 of PTX-M and Taxol were 55.77% and 40.38%, respectively. Although there were no significant differences between two groups, the TIR of micelle was a little higher than that of Taxol. This slightly enhanced anti-tumor activity of the PTX-M could be explained by the increased local concentration of PTX near the tumor via EPR effect (Torchilin, 2010). This phenomenon was also reported in some other polymeric micelle literature. After micelle injected into blood circulation, the drug encapsulated in micelle might quickly distribute into tumor through EPR effect. Although Taxol could stay in the blood for a long time, it could not enter into tumors better and the final fate of PTX in Taxol was to distribute to the liver, spleen, and lung slowly. As the tissue distribution experiment showed, the accumulation amount of Taxol in the liver and lung was higher than PTX-M.

In histological observations of tumor HE sections (Figure 6), many tumor cells were HE stained and no abnormality was found in the saline group (Figure 6a) and OCCC-blank group (Figure 6b). Abnormalities in PTX-M (Figure 6c) and Taxol group (Figure 6d) compared with the saline control group were seen, HE staining was much slighter, indicating that there were a lot of tumor cells that died.

Conclusion

In this study, a micelle delivery system based on a novel pH-sensitive graft copolymer of *N*-octyl-*N*-(2-carboxyl-cyclohexamethenyl) chitosan derivatives was compared with Taxol as the delivery system of PTX. Pharmacokinetics showed longer $t_{1/2\beta}$ and larger V_d than Taxol, which demonstrated that micelle was distributed to tissue from blood easily. The NIR-imaging study and tissue distribution demonstrated that PTX-M was widely distributed into most tissues, most of them found in the liver, spleen, and lung, which was attributed to the uptake by RES. Moreover, there was a lower concentration of PTX in the heart, spleen, and lung that might reduce the side-effects of anti-tumor drugs in these tissues. PTX-M exhibited a more enhanced anti-

tumor activity than Taxol; this might be attributed to the increased local concentration of PTX near the tumor via EPR effect. In contrast to Taxol, these results indicated that PTX-M formulation might be the better possible approach which would bypass the limitations of poor water-solubility PTX, and was expected to be a potential PTX delivery system.

Declaration of interest

This study is financially supported by the National Natural Science Foundation of China (30772662), Natural Science Foundation of Jiangsu, China (BK2009304), Major Program for New Drug Discovery (2009ZX09310-004, 2009ZX09503-028), and PhD Programs Foundation of Ministry of Education of China (20090096110005).

References

Bae, Y., Diezi, T.A., Zhao, A., Kwon, G.S. (2007). Mixed polymeric micelles for combination cancer chemotherapy through the concurrent delivery of multiple chemotherapeutic agents. J Contr Rel. 122:324–30.

Chen, H., Wang, Y., Xu, J., Ji, J., Zhang, J., Hu, Y., Gu, Y. (2008). Non-invasive near infrared fluorescence imaging of CdHgTe quantum dots in mouse model. J Fluoresc. 18:801–11.

Cho, Y.W., Park, S.A., Han, T.H., Son, D.H., Park, J.S., Oh, S.J., Moon, D.H., Cho, K.J., Ahn, C.H., Byun, Y., Kim, I.S., Kwon, I.C., Kim, S.Y. (2007). In vivo tumor targeting and radionuclide imaging with self-assembled nanoparticles: mechanisms, key factors, and their implications. Biomaterials. 28:1236–47.

Crosasso, P., Ceruti, M., Brusa, P., Arpicco, S., Dosio, F., Cattel, L. (2000). Preparation, characterization and properties of sterically stabilized paclitaxel-containing liposomes. J Contr Rel. 63:19–30.

Danson, S., Ferry, D., Alakhov, V., Margison, J., Kerr, D., Jowle, D., Brampton, M., Halbert, G., Ranson, M. (2004). Phase I dose escalation and pharmacokinetic study of pluronic polymer-bound doxorubicin (SP1049C) in patients with advanced cancer. Br J Cancer. 90;2085–91.

Desai, N., Trieu, V., Yao, Z., Louie, L., Ci, S., Yang, A., Tao, C., De, T., Beals, B., Dykes, D., Noker, P., Yao, R., Labao, E., Hawkins, M., Soon-Shiong, P. (2006). Increased antitumor activity, intratumor paclitaxel concentrations, and endothelial cell transport of cremophor-free, albumin-bound paclitaxel, ABI-007, compared with cremophor-based paclitaxel. Clin Cancer Res. 12:1317–24.

Dhanikula, A.B., Singh, D.R., Panchagnula, R. (2005). In vivo pharmacokinetic and tissue distribution studies in mice of alternative formulations for local and systemic delivery of Paclitaxel: gel, film, prodrug, liposomes and micelles. Curr Drug Deliv. 2:35–44.

Hruby, M., Konak, C., Ulbrich, K. (2005). Polymeric micellar pH-sensitive drug delivery system for doxorubicin. J Contr Rel. 103:137–48.

Huh, K.M., Lee, S.C., Cho, Y.W., Lee, J., Jeong, J.H., Park, K. (2005). Hydrotropic polymer micelle system for delivery of paclitaxel. J Contr Rel. 101:59–68.

Huh, K.M., Min, H.S., Lee, S.C., Lee, H.J., Kim, S., Park, K. (2008). A new hydrotropic block copolymer micelle system for aqueous solubilization of paclitaxel. J Contr Rel. 126:122–9.

Huo, M., Zhang, Y., Zhou, J., Zou, A., Yu, D., Wu, Y., Li, J., Li, H. (2010). Synthesis and characterization of low-toxic amphiphilic chitosan derivatives and their application as micelle carrier for antitumor drug. Int J Pharmaceut. 394:162–73.

Ibrahim, N.K., Desai, N., Legha, S., Soon-Shiong, P., Theriault, R.L., Rivera, E., Esmaeli, B., Ring, S.E., Bedikian, A., Hortobagyi, G.N., Ellerhorst, J.A. (2002). Phase I and pharmacokinetic study of ABI-007, a Cremophor-free, protein-stabilized, nanoparticle formulation of paclitaxel. Clin Cancer Res. 8:1038–44.

Ibrahim, N.K., Samuels, B., Page, R., Doval, D., Patel, K.M., Rao, S.C., Nair, M.K., Bhar, P., Desai, N., Hortobagyi, G.N. (2005). Multicenter phase II trial of ABI-007, an albumin-bound paclitaxel, in women with metastatic breast cancer. J Clin Oncol. 23:6019–26.

Kim, S.C., Kim, D.W., Shim, Y.H., Bang, J.S., Oh, H.S., Wan Kim, S., Seo, M.H. (2001). In vivo evaluation of polymeric micellar paclitaxel formulation: toxicity and efficacy. J Contr Rel. 72:191–202.

Kwon, G.S. (2003). Polymeric micelles for delivery of poorly water-soluble compounds. Crit Rev Ther Drug Carrier Syst. 20:357–3.

Kwon, G.S., Yokoyama, M., Okano, T., Sakurai, Y., Kataoka, K. (1993). Biodistribution of micelle-forming polymer-drug conjugates. Pharm Res. 10:970–4.

Lee, A.L., Wang, Y., Cheng, H.Y., Pervaiz, S., Yang, Y.Y. (2009). The co-delivery of paclitaxel and Herceptin using cationic micellar nanoparticles. Biomaterials. 30:919–27.

Lee, E.S., Gao, Z., Kim, D., Park, K., Kwon, I.C., Bae, Y.H. (2008). Super pH-sensitive multifunctional polymeric micelle for tumor pH(e) specific TAT exposure and multidrug resistance. J Contr Rel. 129:228–36.

Li, H., Liu, J., Ding, S., Zhang, C., Shen, W., You, Q. (2009). Synthesis of novel pH-sensitive chitosan graft copolymers and micellar solubilization of paclitaxel. Int J Biol Macromol. 44:249–56.

Liggins, R.T., Burt, H.M. (2004). Paclitaxel-loaded poly(L-lactic acid) microspheres 3: blending low and high molecular weight polymers to control morphology and drug release. Int J Pharm. 282:61–71.

Liu, J., Li, H., Jiang, X., Zhang, C., Ping, Q. (2010). Novel pH-sensitive chitosan-derived micelles loaded with paclitaxel. Carbohydr Polym. 82:432–9.

Matsumoto, J., Nakada, Y., Sakurai, K., Nakamura, T., Takahashi, Y. (1999). Preparation of nanoparticles consisted of poly(L-lactide)-poly(ethylene glycol)-poly(L-lactide) and their evaluation in vitro. Int J Pharm. 185:93–101.

Matsumura, Y., Hamaguchi, T., Ura, T., Muro, K., Yamada, Y., Shimada, Y., Shirao, K., Okusaka, T., Ueno, H., Ikeda, M., Watanabe, N. (2004). Phase I clinical trial and pharmacokinetic evaluation of NK911, a micelle-encapsulated doxorubicin. Br J Cancer. 91:1775–81.

Mizumura, Y., Matsumura, Y., Yokoyama, M., Okano, T., Kawaguchi, T., Moriyasu, F., Kakizoe, T. (2002). Incorporation of the anticancer agent KRN5500 into polymeric micelles diminishes the pulmonary toxicity. Jpn J Cancer Res. 93:1237–43.

Ooya, T., Lee, J., Park, K. (2003). Effects of ethylene glycol-based graft, star-shaped, and dendritic polymers on solubilization and controlled release of paclitaxel. J Contr Rel. 93:121–7.

Qu, G., Yao, Z., Zhang, C., Wu, X., Ping, Q. (2009). PEG conjugated N-octyl-O-sulfate chitosan micelles for delivery of paclitaxel: in vitro characterization and in vivo evaluation. Eur J Pharm Sci. 37:98–105.

Rapoport, N. (2007). Physical stimuli-responsive polymeric micelles foranti-cancer drug delivery. Prog Polym Sci. 32:962–90.

Rowinsky, E.K., Donehower, R.C. (1993). The clinical pharmacology of paclitaxel (Taxol). Semin Oncol. 2016–25.

Sawant, R.R., Torchilin, V.P. (2009). Enhanced cytotoxicity of TATp-bearing paclitaxel-loaded micelles in vitro and in vivo. Int J Pharm. 374:114–8.

Sawant, R.R., Vaze, O., Rockwell, K., Torchilin, V.P. (2010). Palmitoyl ascorbate-modified liposomes as nanoparticle platform for ascorbate-mediated cytotoxicity and paclitaxel co-delivery. Eur J Pharm Biopharm. 75:321-326

Sonnichsen, D.S., Relling, M.V. (1994). Clinical pharmacokinetics of paclitaxel. Clin Pharmacokinet. 27:256–69.

Spencer, C.M., Faulds, D. (1994). Paclitaxel. A review of its pharmacodynamic and pharmacokinetic properties and therapeutic potential in the treatment of cancer. Drugs. 48:794–847.

Szebeni, J., Muggia, F.M., Alving, C.R. (1998). Complement activation by Cremophor EL as a possible contributor to hypersensitivity

to paclitaxel: an in vitro study. J Natl Cancer Inst. 90: 300–6.
Torchilin, V. (2010). Tumor delivery of macromolecular drugs based on the EPR effect. Adv Drug Deliv Rev. (In press).
Torchilin, V.P. (2001). Structure and design of polymeric surfactant-based drug delivery systems. J Contr Rel. 73:137–72.
Torchilin, V.P. (2007). Micellar nanocarriers: pharmaceutical perspectives. Pharm Res. 24:1–16.
van Zuylen, L., Karlsson, M.O., Verweij, J., Brouwer, E., de Bruijn, P., Nooter, K., Stoter, G., Sparreboom, A. (2001). Pharmacokinetic modeling of paclitaxel encapsulation in Cremophor EL micelles. Cancer Chemother Pharmacol. 47:309–18.
Wanjun, T., Cunxin, W., Donghua, C. (2005). Kinetic studies on the pyrolysis of chitin and chitosan. Polymer Degr Stab. 87:389–94.
Xie, Z., Guan, H., Chen, X., Lu, C., Chen, L., Hu, X., Shi, Q., Jing, X. (2007). A novel polymer-paclitaxel conjugate based on amphiphilic triblock copolymer. J Contr Rel. 117:210–6.
Yang, T., Choi, M.K., Cui, F.D., Kim, J.S., Chung, S.J., Shim, C.K., Kim, D.D. (2007). Preparation and evaluation of paclitaxel-loaded PEGylated immunoliposome. J Contr Rel. 120: 169–77.
Yokoyama, M., Miyauchi, M., Yamada, N., Okano, T., Sakurai, Y., Kataoka, K., Inoue, S. (1990). Characterization and anticancer activity of the micelle-forming polymeric anticancer drug adriamycin-conjugated poly(ethylene glycol)-poly(aspartic acid) block copolymer. Cancer Res. 50:1693–700.
Yokoyama, M., Okano, T., Sakurai, Y., Ekimoto, H., Shibazaki, C., Kataoka, K. (1991). Toxicity and antitumor activity against solid tumors of micelle-forming polymeric anticancer drug and its extremely long circulation in blood. Cancer Res. 51: 3229–36.
Zhang, C., Ping, Q., Zhang, H., Jian, S. (2003). Preparation of N-alkyl-O-sulfate chitosan derivatives and micellar solubilization of taxol. Carbohydr Polymers. 54:137–44.
Zhang, C., Qu, G., Sun, Y., Wu, X., Yao, Z., Guo, Q., Ding, Q., Yuan, S., Shen, Z., Ping, Q., Zhou, H. (2008a). Pharmacokinetics, biodistribution, efficacy and safety of N-octyl-O-sulfate chitosan micelles loaded with paclitaxel. Biomaterials. 29:1233–41.
Zhang, C., Qu, G., Sun, Y., Yang, T., Yao, Z., Shen, W., Shen, Z., Ding, Q., Zhou, H., Ping, Q. (2008b). Biological evaluation of N-octyl-O-sulfate chitosan as a new nano-carrier of intravenous drugs. Eur J Pharm Sci. 33:415–23.
Zhang, J., Chen, H., Xu, L., Gu, Y. (2008c). The targeted behavior of thermally responsive nanohydrogel evaluated by NIR system in mouse model. J Contr Rel. 131:34–40.
Zhang, Y., Tang, L., Sun, L., Bao, J., Song, C., Huang, L., Liu, K., Tian, Y., Tian, G., Li, Z., Sun, H., Mei, L. (2010). A novel paclitaxel-loaded poly(epsilon-caprolactone)/Poloxamer 188 blend nanoparticle overcoming multidrug resistance for cancer treatment. Acta Biomater. 6:2045–52.
Zhang, Z., Feng, S.S. (2006). The drug encapsulation efficiency, in vitro drug release, cellular uptake and cytotoxicity of paclitaxel-loaded poly(lactide)-tocopheryl polyethylene glycol succinate nanoparticles. Biomaterials. 27:4025–33.
Zhu, C., Jung, S., Luo, S., Meng, F., Zhu, X., Park, T.G., Zhong, Z. (2010). Co-delivery of siRNA and paclitaxel into cancer cells by biodegradable cationic micelles based on PDMAEMA-PCL-PDMAEMA triblock copolymers. Biomaterials. 31:2408–16.